AIAA SciTech Forum
7-11 January 2019, San Diego, California
AIAA Scitech 2019 Forum

10.2514/6.2019-1848

Drag Minimization of Co-Flow Jet Control Surfaces at Cruise Conditions

Kewei Xu *, Jinhuan Zhang †, Gecheng Zha ‡
Dept. of Mechanical and Aerospace Engineering
University of Miami, Coral Gables, Florida 33124
E-mail: gzha@miami.edu

Abstract

This paper numerically investigates drag minimization techniques of the CFJ control surface when it is not activated at cruise condition. Three methods are studied to minimize the control surface drag. One is to let the CFJ produce a very light jet at the airfoil surface to decrease the drag at a low power. This method is effective at various cruise Mach numbers. Compared with the baseline, it decreases the corrected drag coefficient ($(C_D)_c$) by 11.4%, 13.0% and 14.6% at Ma_∞=0.15, 0.45 and 0.7. The second method is to cover the injection and suction slot with a small movable surface segment and turn the CFJ off at cruise. This brings the C_D of CFJ airfoil to the same level as the baseline airfoil. The third method is to simply turn the micro-compressor actuator off and leave the CFJ ducts open with no jet. This method does increase the drag. As a result of the increased lift coefficient that allows reducing the control surface area, the overall drag of the control surface will be significantly decreased to benefit the aircraft system.

Nomenclature

CFJ	Co-flow jet
AoA	Angle of attack
AFC	Active Flow Control
C	Chord length
C_L	Lift coefficient
C_D	Drag coefficient
$(C_D)_c$	Drag coefficient corrected for CFJ airfoil
C_Lmax	Maximum lift coefficient
C_M	Moment coefficient
C_p	Constant pressure specific heat
C_RW	Aircraft Productivity parameter
c_t	Engine cruise thrust specific fuel consumption [fuel weight (N)/(thrust(N) s)]
C_μ	Jet momentum coef. $\dot{m}_j\, U_j/(q_\infty\, S)$
D	Total drag on the airfoil
$FASIP$	Flow-Acoustics-Structure Interaction Package
H_t	Total enthalpy

* Ph.D. Student
† Visiting Student
‡ Professor, ASME Fellow, AIAA associate Fellow

L	Total lift on the airfoil
LE	Leading Edge
C	Chord length
$\dot{m}$	Mass flow
Ma	Mach number
Ma_∞	Cruise Mach number
P	CFJ Pumping power
P_c	Power coefficient $L/(q_\infty S V_\infty)$
PR	Total pressure ratio, Γ
P_t	Total pressure
R	Aircraft range
$RANS$	Reynolds-Averaged Navier-Stokes
R_e	Reynolds number
S	Planform area of the wing
TE	Trailing Edge
T_t	Total temperature
$\bar{W}$	Aircraft averaged weight during cruise
W_0	Aircraft initial gross weight at takeoff
W_f	Final weight at landing
V_∞	Freestream velocity
$ZNMF$	Zero-Net Mass Flux
C_L/C_D	Aerodynamic efficiency
$(C_L/C_D)_c$	Aerodynamic efficiency corrected for CFJ airfoil
(C_L^2/C_D)	Productivity efficiency coefficient
$(C_L^2/C_D)_c$	Productivity efficiency coefficient corrected for CFJ airfoil
c	Subscript, stands for corrected
j	Subscript, stands for jet
α	Angle of attack
β	Sideslip angle
γ	Air specific heats ratio
η	CFJ pumping system efficiency, propeller efficiency
ρ_∞	Freestream density
δ	Deflection angle
θ_1	Angle between the injection slot surface and a line normal to the airfoil chord
θ_2	Angle between the suction slot surface and a line normal to the airfoil chord

1 Introduction

Aircraft stability are maintained through control surfaces such as vertical tails, horizontal tails and canards. Control surfaces are required to have high control authority by generating sufficient lift with rapid response time to keep the aircraft trimmed. To achieve such performance, the control surfaces usually have large sizes, which bring severe penalty of weight, drag and energy consumption. Active Flow control (AFC) as means to enhance lift has great potential to reduce the size and weight of control surfaces [1, 2, 3, 4, 5, 6, 7]. Vertical tails using sweeping jets and synthetic jets AFC were studied by Boeing and NASA in [8, 9, 10, 11, 12, 13, 14, 15]. Nicholas et.al conducted wind tunnel experiments on a swept back, tapered tail with a 29.6% chord rudder [8]. Using flow

control, the side force was increased by up to 18% at moderate rudder deflections with a momentum coefficient C_μ=0.721%. Compared with synthetic jets, sweeping jets have higher C_μ output and corresponding jet velocity. Thus sweeping jets were selected over the synthetic jets by Boeing/NASA team for the subsequent full-scale AFC wind tunnel tests [9, 10].

The rudder with sweeping jet AFC were tested on sub-scale [11, 12], full-scale models [9, 10] and finally in flight [9]. The sub-scale test was performed at a 14% scale model of Caltech and more than 50% side force enhancement were achieved by sweeping jet actuation with the momentum coefficient C_μ of 1.7%. The full-scale vertical tail model equipped with sweeping jet AFC was tested at a nominal speed of 100 knots ($M_\infty \sim 0.15$, Re $\sim$ 15 million), a maximum speed of 130 knots ($M_\infty \sim 0.2$, Re $\sim$ 20 million) and across the vertical tail flight envelop for rudder deflections (0° to 30°) and sideslip angles (0° to −7.5°). A 31-actuator AFC configuration produces significant flow attachment on the rudder, which results in 20% increase in side force for the maximum rudder deflection of 30° at 0 and −7.5° sideslip angles. Subsequently, the sweeping jet-enhanced vertical tail was flown on the Boeing 757 ecoDemonstrator in the spring of 2015. A side force increase of 13% to 16% was estimated at 30° rudder deflection for critical sideslip range between $\beta = 0°$ and −7.5° with the activation of AFC. Kara analyzed the complex flow inside the sweeping jet for design optimization of actuator geometry with minimum pressure loss [16, 17]. However, these studies [8, 9, 10, 11, 12, 13, 14, 15, 16, 17] do not report sufficient results on energy expenditure of the sweeping jets, which tend to suffer large energy loss due to jet sweeping, turning, and flow separation. Furthermore, the system energy penalty due to introducing the air flow mass from engine bleed is not given.

Recently, Zhang et al [18] conducted 2D numerical simulation to study high control authority aircraft control surfaces using Co-Flow Jet (CFJ) airfoil [2, 5, 19, 20, 21, 22, 23, 24, 25, 26, 27, 28], which is a zero-net mass flux (ZNMF) flow control that does not need to use engine bleed. Xu et al [29] applied the CFJ flow control to a 3D vertical tail, which demonstrates a very high control authority enhancement. A small C_μ of 0.025 generates a 28% C_L increase at 0° sideslip angle. At the same time, it achieves a higher corrected aerodynamic efficiency ($(C_L/C_D)_c$) than the baseline case. With C_μ of 0.26, the C_L of the 3D vertical tail is increased 99.25% at 0° sideslip angle. Both the 2D and 3D studies demonstrate the high effectiveness of CFJ control surfaces. However, one issue not addressed in [18] and [29] is how to deal with the CFJ slots when the control surface is not in use at cruise conditions. The existence of the slots without jet may increase the drag even though the slots size is usually very small.

The objective of this paper is to study the following three methods for minimizing the CFJ control surface drag when it is not in use at cruise condition: 1) use a very light jet at cruise; 2) cover the slots using a small moving surface segment. 3) turn the micro-compressor actuator off and leave the CFJ ducts open. For the method 1, the light jet is intended to reduce the drag at a very low energy cost to make the overall equivalent drag coefficient no greater than the baseline control surface. The method 2 is intended to restore the drag coefficient of the CFJ control surface to the level of the baseline by a mechanical system instead of jet. The method 3 is to simply turn the micro-compressor actuator off and leave the CFJ ducts open with no jet, which is the simplest method. Before studying the CFJ control surface at cruise conditions, the CFJ control surface designed in [18] is further optimized using trade study by varying the injection location and size.

1.1 The Control Surface Co-Flow Jet Airfoil

In a CFJ airfoil, an injection slot near leading edge (LE) and a suction slot near trailing edge (TE) on the airfoil suction surface are created as sketched in Fig. 1. A small amount of mass flow is withdrawn into the airfoil near the TE, pressurized and energized by a micro-compressor inside the airfoil, and injected near the LE in the direction tangent to the main flow. The whole process does not add any mass flow to the system and hence is a

ZNMF flow control. In addition, the required CFJ energy expenditure is very low. This is because the injection is near the suction peak of the airfoil where the lowest main flow pressure is located, and the jet suction is near the trailing edge where the highest main flow pressure is located.

A symmetric CFJ airfoil with no flap is used as the control surface configuration in this study as shown in Fig. 2. The injection slot and the suction slot are distributed on both sides of control surface CFJ airfoil. When one side CFJ is working to generate lift, the other side CFJ is closed. In the first part of this paper on optimizing the control surface, the closed slots are treated as steps, which bring a small penalty to the lift and more penalty to the drag. In the second part of the paper on minimizing the drag coefficient at cruise condition, three different aforementioned methods are studied to deal with the slots when the control surface is not in use.

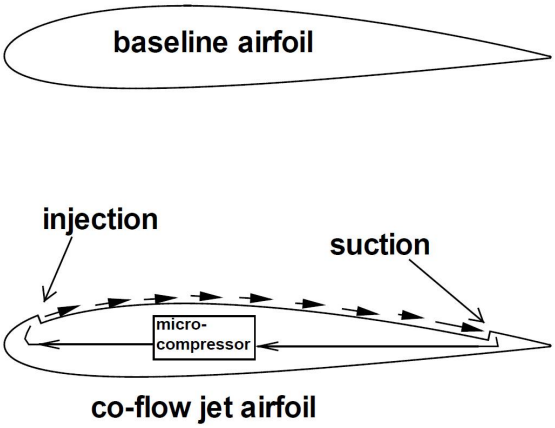

Figure 1: Baseline airfoil and CFJ airfoil.

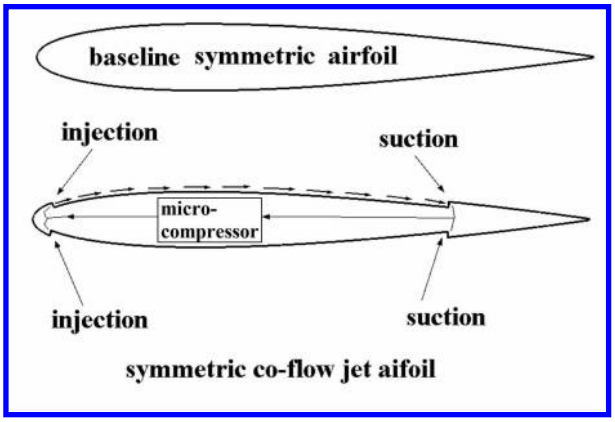

Figure 2: Baseline symmetric airfoil and symmetric CFJ airfoil.

2 CFJ Parameters

This section lists the important parameters used to evaluate aerodynamic performance of a CFJ airfoil.

2.1 Jet Momentum Coefficient

The jet momentum coefficient C_μ is a parameter used to quantify the jet intensity. It is defined as:

$$C_\mu = \frac{\dot{m} V_j}{\frac{1}{2}\rho_\infty {V_\infty}^2 S} \tag{1}$$

where $\dot{m}$ is the injection mass flow, V_j is the mass-averaged injection velocity, ρ_∞ and V_∞ denote the free stream density and velocity, and S is the planform area.

2.2 Lift and Drag Calculation

For CFD simulation, the full reactionary force produced by the momentum and pressure at the injection and suction slots are included by using control volume analysis. Zha et al.[30] give the following formulations to

calculate the lift and drag due to the jet reactionary force for a CFJ airfoil. By considering the effects of injection and suction jets on the CFJ airfoil, the expressions for these reactionary forces are given as :

$$F_{x_{cfj}} = (\dot{m}_j V_{j1} + p_{j1} A_{j1}) * cos(\theta_1 - \alpha) - (\dot{m}_j V_{j2} + p_{j2} A_{j2}) * cos(\theta_2 + \alpha) \tag{2}$$

$$F_{y_{cfj}} = (\dot{m}_{j1} V_{j1} + p_{j1} A_{j1}) * sin(\theta_1 - \alpha) + (\dot{m}_{j2} V_{j2} + p_{j2} A_{j2}) * sin(\theta_2 + \alpha) \tag{3}$$

where the subscripts 1 and 2 stand for the injection and suction respectively, and θ_1 and θ_2 are the angles between the injection and suction slot's surface and a line normal to the airfoil chord. α is the angle of attack.

The total lift and drag on the airfoil can then be expressed as:

$$D = R'_x - F_{x_{cfj}} \tag{4}$$

$$L = R'_y - F_{y_{cfj}} \tag{5}$$

where R'_x and R'_y are the surface integral of pressure and shear stress in x (drag) and y (lift) direction excluding the internal ducts of injection and suction. For CFJ wing simulations, the total lift and drag are calculated by integrating Eqs.(4) and (5) in the spanwise direction.

2.3 Power Coefficient

CFJ is implemented by mounting a pumping system inside the wing that withdraws air from the suction slot and blows it into the injection slot. The power consumption is determined by the jet mass flow and total enthalpy change as the following:

$$P = \dot{m}(H_{t1} - H_{t2}) \tag{6}$$

where H_{t1} and H_{t2} are the mass-averaged total enthalpy in the injection cavity and suction cavity respectively, P is the Power required by the pump and $\dot{m}$ the jet mass flow rate. Introducing P_{t1} and P_{t2} the mass-averaged total pressure in the injection and suction cavity respectively, the pump efficiency η, and the total pressure ratio of the pump $\Gamma = \frac{P_{t1}}{P_{t2}}$, the power consumption is expressed as:

$$P = \frac{\dot{m} C_p T_{t2}}{\eta} (\Gamma^{\frac{\gamma-1}{\gamma}} - 1) \tag{7}$$

where γ is the specific heat ratio equal to 1.4 for air. The power coefficient is expressed as:

$$P_c = \frac{P}{\frac{1}{2}\rho_\infty V_\infty^3 S} \tag{8}$$

2.4 Corrected Aerodynamic Efficiency

The conventional wing aerodynamic efficiency is defined as:

$$\frac{L}{D} \tag{9}$$

For the CFJ wing, the ratio above still represents the pure aerodynamic relationship between lift and drag. However since CFJ active flow control consumes energy, the ratio above is modified to take into account the energy consumption of the pump. The formulation of the corrected aerodynamic efficiency for CFJ wings is:

$$(\frac{L}{D})_c = \frac{C_L}{C_D + P_c} \tag{10}$$

where V_∞ is the free stream velocity, P is the pumping power, and L and D are the lift and drag generated by the CFJ wing. The formulation above converts the power consumed by the CFJ into a force $\frac{P}{V_\infty}$ which is added to the aerodynamic drag D. If the pumping power is set to 0, this formulation returns to the aerodynamic efficiency of a conventional wing.

3 CFD simulation

The in-house high accuracy CFD code Flow-Acoustics-Structure Interaction Package (FASIP) is used to conduct the numerical simulation. The 2D Reynolds averaged Navier-Stokes (RANS) equations with one-equation Spalart-Allmaras (SA) [32] turbulence model is used. A 5th order WENO scheme for the inviscid flux [33, 34, 35, 36, 37, 38] and a 4th order central differencing for the viscous terms [33, 37] are employed to discretize the Navier-Stokes equations. The low diffusion E-CUSP scheme used as the approximate Riemann solver suggested by Zha et al [34] is utilized with the WENO scheme to evaluate the inviscid fluxes. Implicit time marching method using Gauss-Seidel line relaxation is used to achieve a fast convergence rate [38]. Parallel computing is implemented to save wall clock simulation time [39]. The RANS solver is intensively validated for CFJ airfoil simulations [5, 40, 41, 42].

4 Results and Discussion

The mesh independence study for both the baseline NACA0012 and the CFJ-NACA0012 airfoil are conducted at [18]. The same mesh size and topology used in [18] is adopted in this paper.

4.1 Trade Study to Optimize Control Surface Efficiency

The control surface CFJ airfoil (CFJ-NACA0012) configurations are created from the baseline NACA0012 airfoil by translating the suction surface downward, which is defined as the suction surface translation (SST). As described in [18], both sides of the symmetric airfoil have the same slot configuration. However, the co-flow jet is only applied on one side to create lift for the control surface. Fig. 3 and 4 show the CFJ control surfaces with a plain flap.

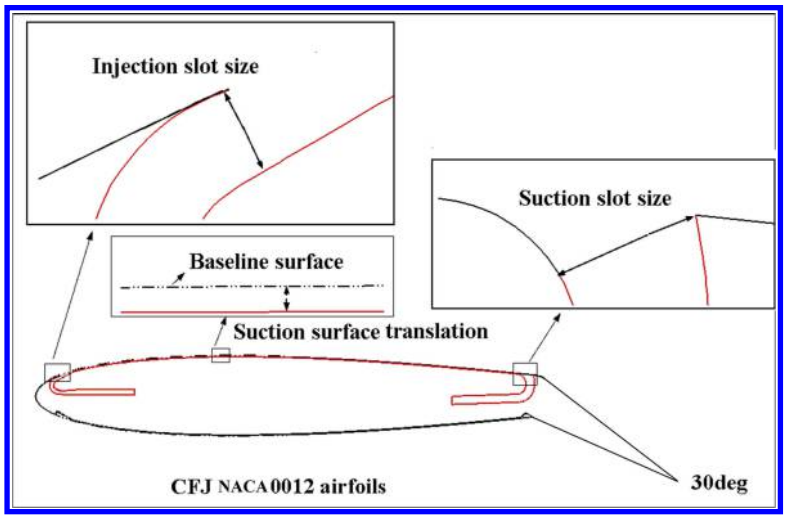

Figure 3: CFJ-NACA0012 airfoil with flaps geometries.

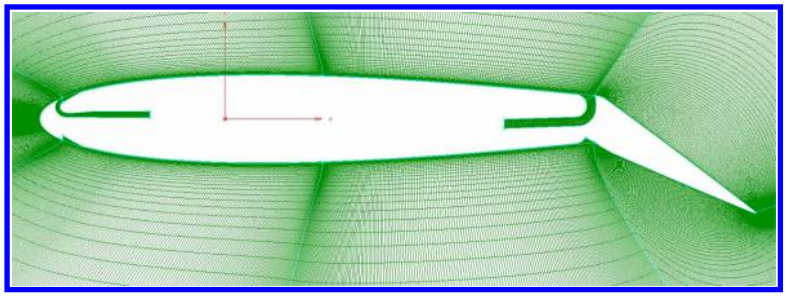

Figure 4: Computational mesh for CFJ-NACA0012 airfoil with flap deflection angle 30°.

4.1.1 Trade Study of Injection Size

The starting point of the trade study is the CFJ control surface obtained by Zhang et al [18]. It has the flap length of 35%C, deflection angle of 30°, injection location at 4%C from leading edge, injection slot size of 0.5%C, and suction slot right upstream of the flap with the size twice larger than the injection size. The injection size trade study examines the size of 0.5%, 0.75%, 0.85%, 1% C with all other geometry parameters fixed. The trade study holds a constraint that the lift coefficient remains the same as the original control surface, while the aerodynamic efficiency $(C_L/C_D)_c$ is optimized. Since the injection size is varied, when the same lift coefficient is obtained, the required C_μ may be different.

Fig. 5, 6 and 7 show the aerodynamic coefficients of different slot size variation with C_μ=0.05, 0.15, 0.25, which include lift, drag and pitching moment coefficient, corrected aerodynamic efficiency, productivity efficiency, and power coefficient. As shown in Fig. 5, the C_L with different slot size is kept about the same. As slot size increases from 0.5% C to 1% C, P_c is decreased as shown in Fig. 5d, 6d and 7d and reaches it's minimum at slot size of 0.85% C. Comparing between the slot size of 0.5% C and 0.85% C, P_c at AoA=0 decreases 19.5%, 41.6% and 37.7% in at C_μ of 0.05, 0.15 and 0.25 respectively. As a result, maximum $(C_L/C_D)_c$ is increased by 186.3%, 51.9% at C_μ=0.05, 0.15, respectively. However, for C_μ of 0.25, even though the C_L is increased by nearly 138.2%, the $(C_L/C_D)_c$ is lower than the baseline due to the substantially increased power coefficient. $(C_L^2/C_D)_c$ is increased by 330.4%, 238.2% and 88.9% at C_μ=0.05, 0.15, 0.25 respectively. The slot size 0.85% C is hence used to achieve the optimum aerodynamic efficiency of $(C_L/C_D)_c$.

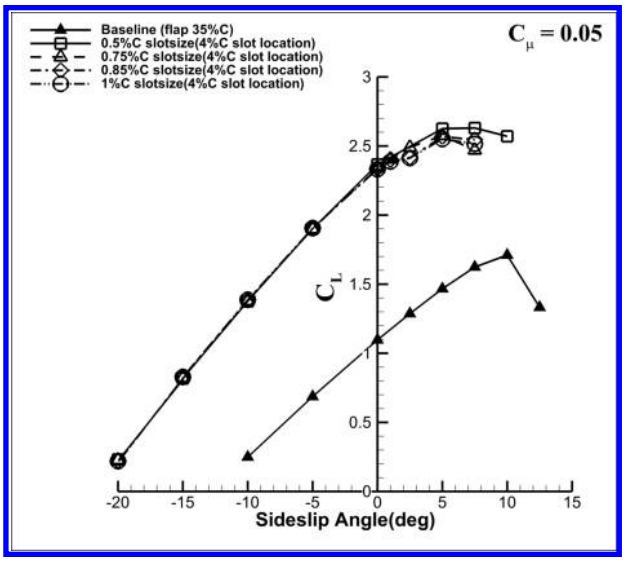

(a) Lift coefficient C_L

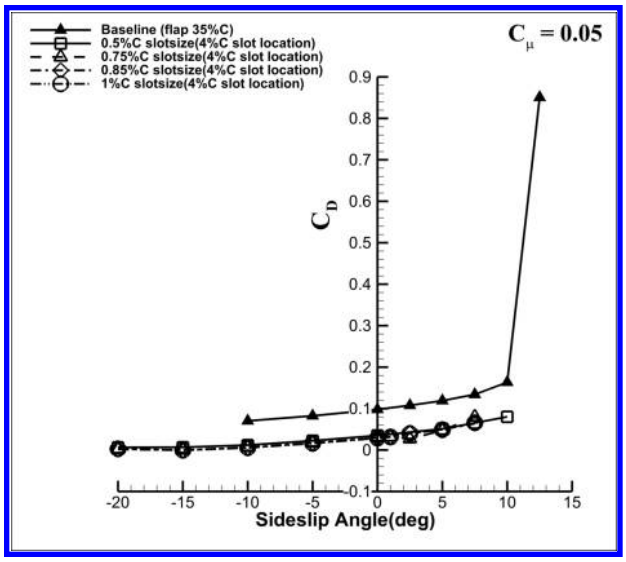

(b) Drag coefficient C_D

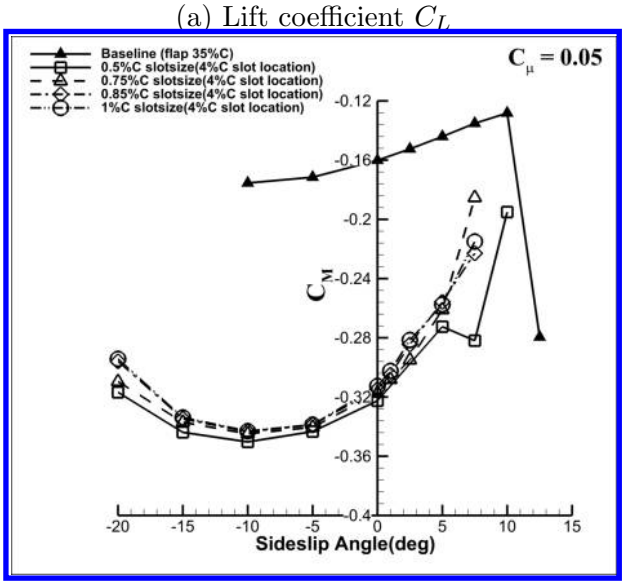

(c) Pitching moment coefficient C_M

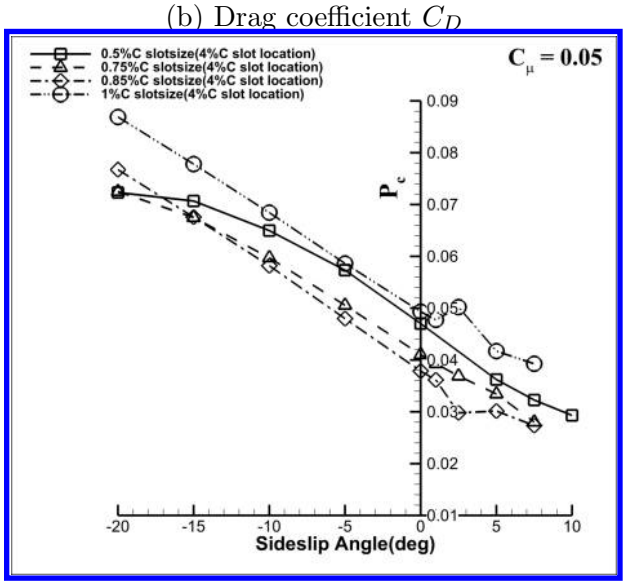

(d) Power coefficient P_c

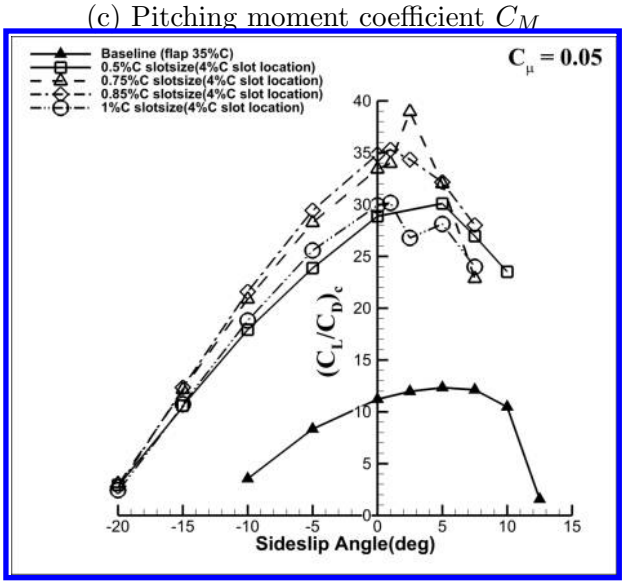

(e) Corrected aerodynamic efficiency $(C_L/C_D)_c$

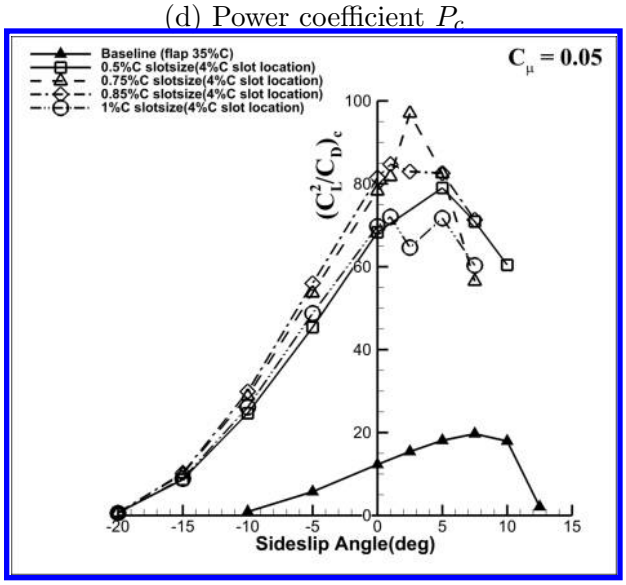

(f)Corrected productivity efficiency coefficient $(C_L^2/C_D)_c$

Figure 5: Aerodynamic coefficients of baseline and CFJ airfoil with injection slot size variation for C_μ=0.05.

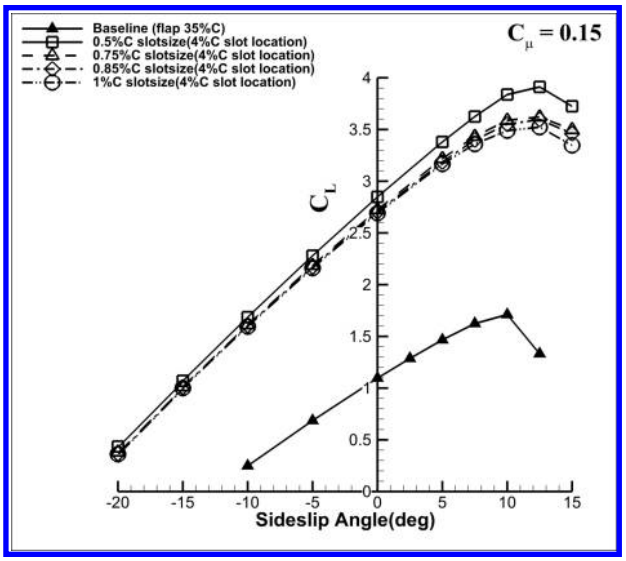

(a) Lift coefficient C_L

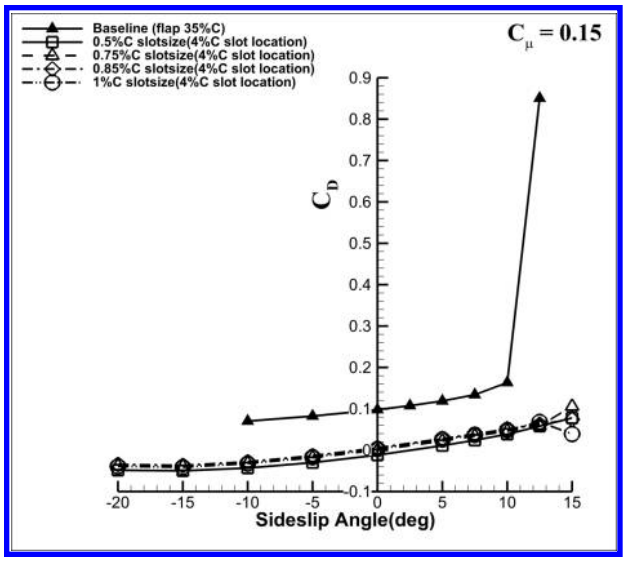

(b) Drag coefficient C_D

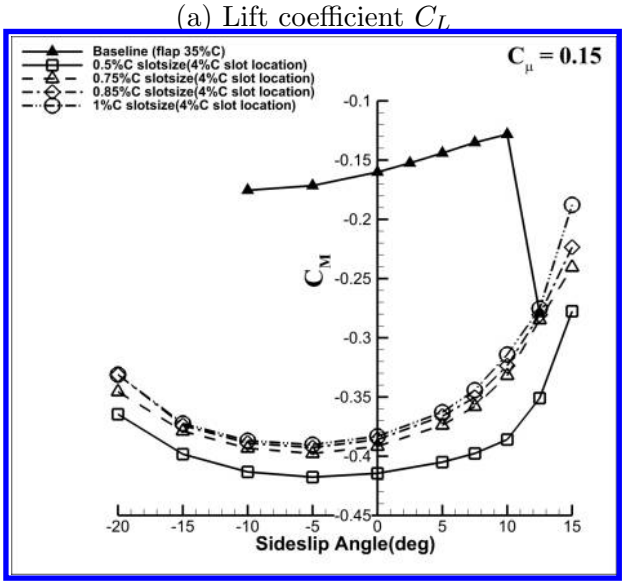

(c) Pitching moment coefficient C_M

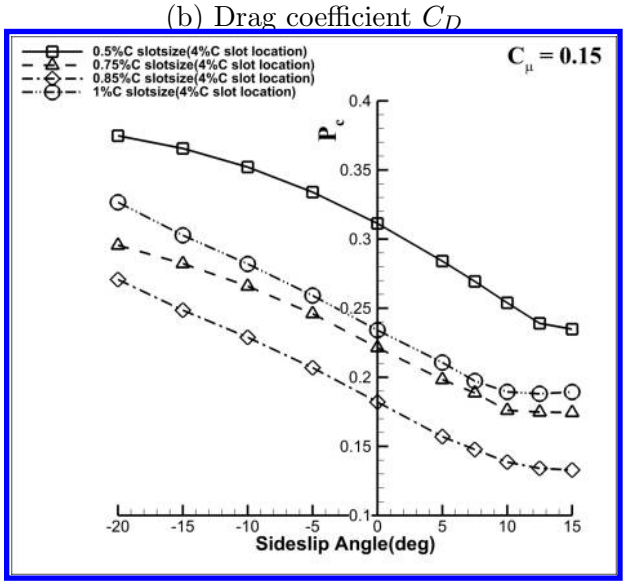

(d) Power coefficient P_c

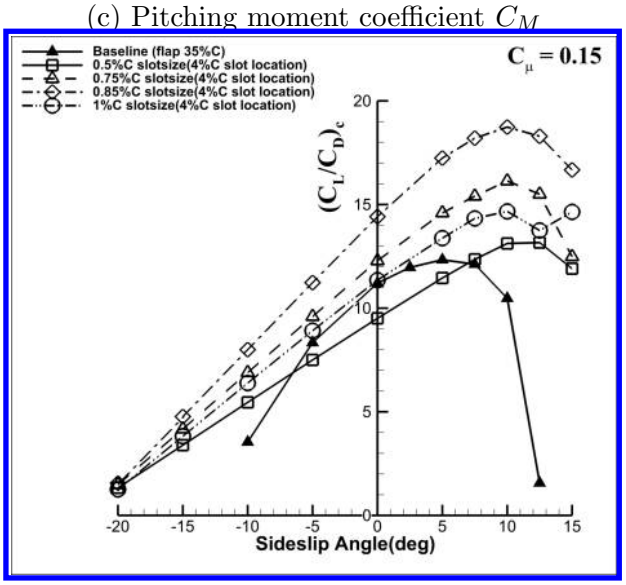

(e) Corrected aerodynamic efficiency $(C_L/C_D)_c$

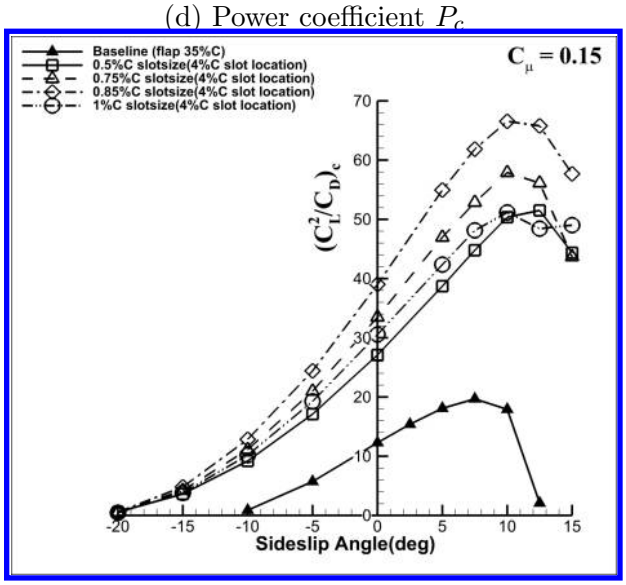

(f)Corrected productivity efficiency coefficient $(C_L^2/C_D)_c$

Figure 6: Aerodynamic coefficients of baseline and CFJ airfoil with injection slot size variation for C_μ=0.15.

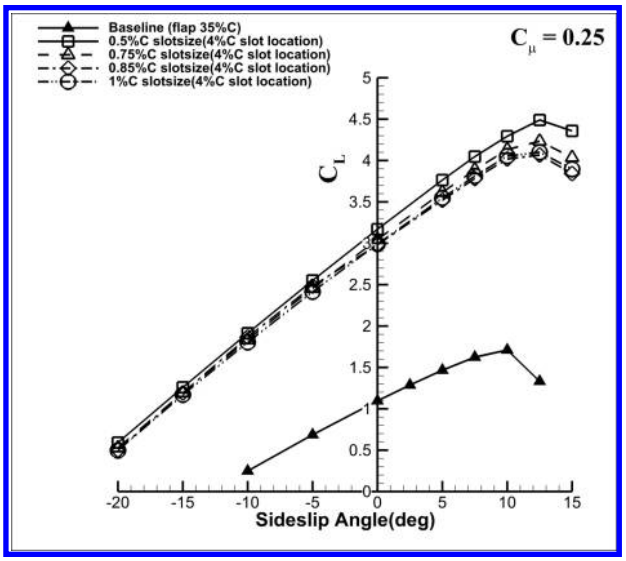

(a) Lift coefficient C_L

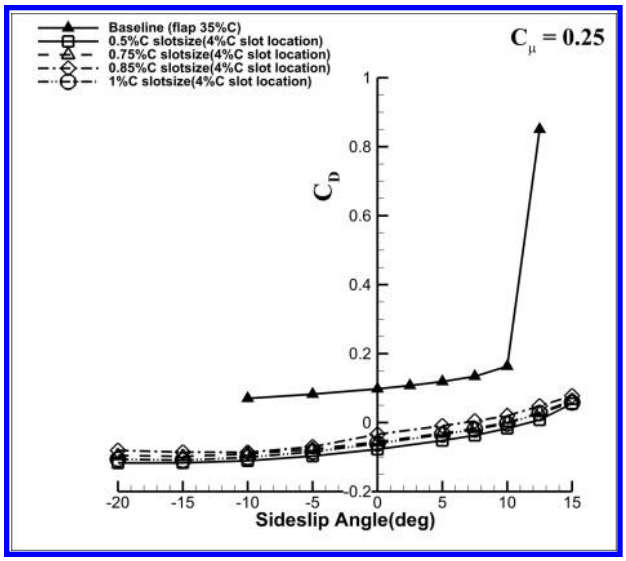

(b) Drag coefficient C_D

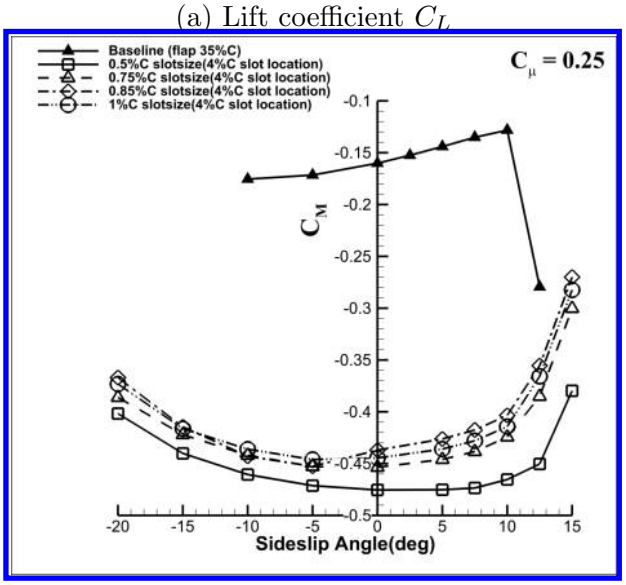

(c) Pitching moment coefficient C_M

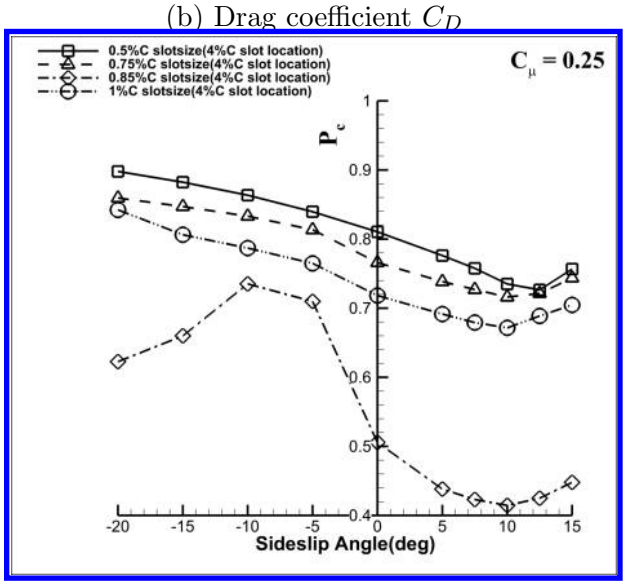

(d) Power coefficient P_c

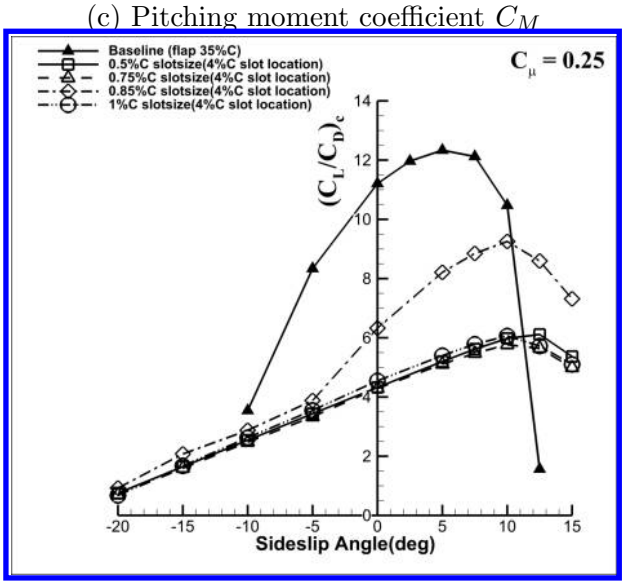

(e) Corrected aerodynamic efficiency $(C_L/C_D)_c$

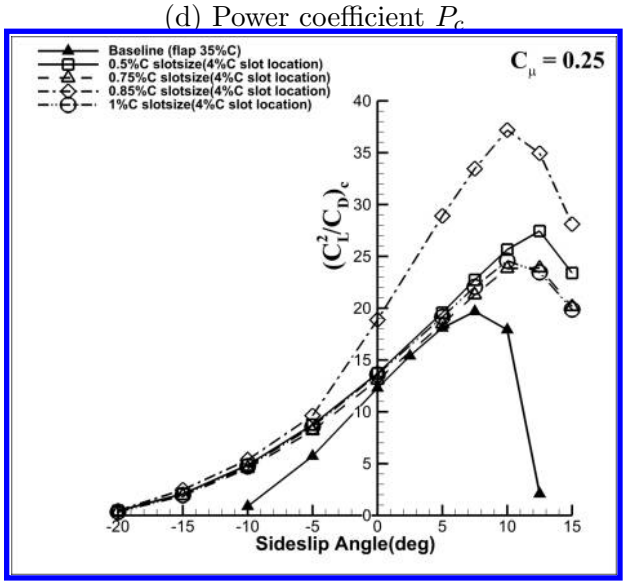

(f)Corrected productivity efficiency coefficient $(C_L^2/C_D)_c$

Figure 7: Aerodynamic coefficients of baseline and CFJ airfoil with injection slot size variation for C_μ=0.25.

4.1.2 Trade Study of Injection Slot Location

This section conducts the trade study of the injection slot location on CFJ control surface aerodynamic efficiency. The control surface of CFJ airfoils have the fixed flap length of 35% C, fixed deflection angle of 30° and injection slot size of 0.85% C. The injection slot location 1%, 1.5%, 2% and 4% C are studied to determine the optimum location. The suction slot size is kept twice larger than the injection slot size of 0.85% C. Fig. 8, 9 and 10 show aerodynamic coefficients variation with sideslip angles for C_μ=0.05, 0.15 and 0.25.

As injection slot location is moved toward the leading edge from 4% to 1% C, P_c is steadily decreased as shown in Fig. 8, 9 and 10 with the minimum P_c achieved at injection slot location at 1.5% C, whereas $(C_L/C_D)_c$ and $(C_L^2/C_D)_c$ reach their maximum. The combination of 0.85% C injection slot size with 1.5% C injection slot location is expected as the optimum configuration. The P_c of 0.85% C injection slot size with 1.5% C injection slot location is reduced by 28.2% and 15.0% at C_μ=0.15 and 0.25 compared with the previous design with injection location at 2% C and slot size 0.5% C conducted by Zhang et al [18]. The reason is that the injection location at 1.5% C benefits most from the low pressure suction peak at leading edge, which only requires a very low power to eject the flow. Compared with baseline control surface with no CFJ, the optimum CFJ control surface has the $(C_L/C_D)_c$ increased by 220.4% and 74.1% respectively at C_μ=0.05 and 0.15. Aerodynamic coefficients comparison between baseline and optimum CFJ control surface are shown in Fig. 11.

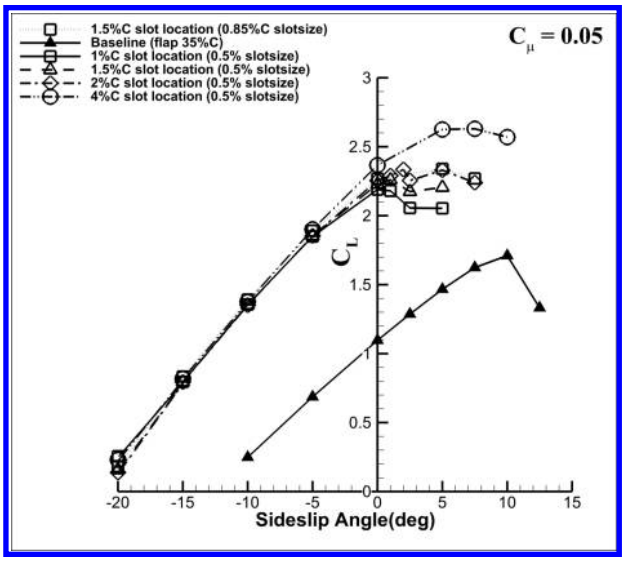

(a) Lift coefficient C_L

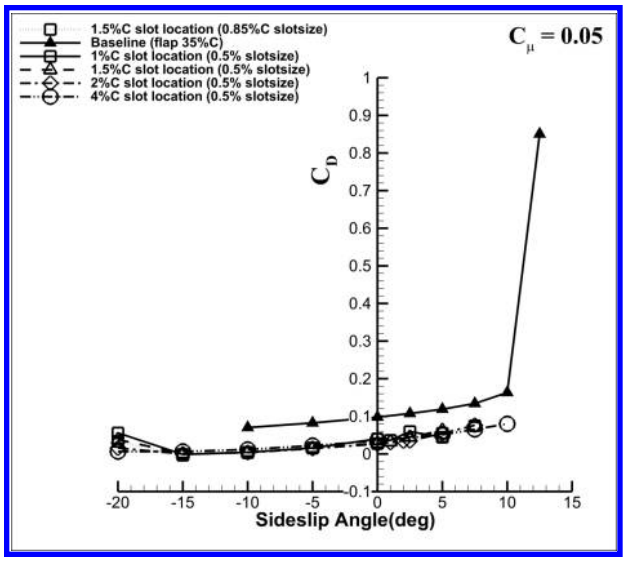

(b) Drag coefficient C_D

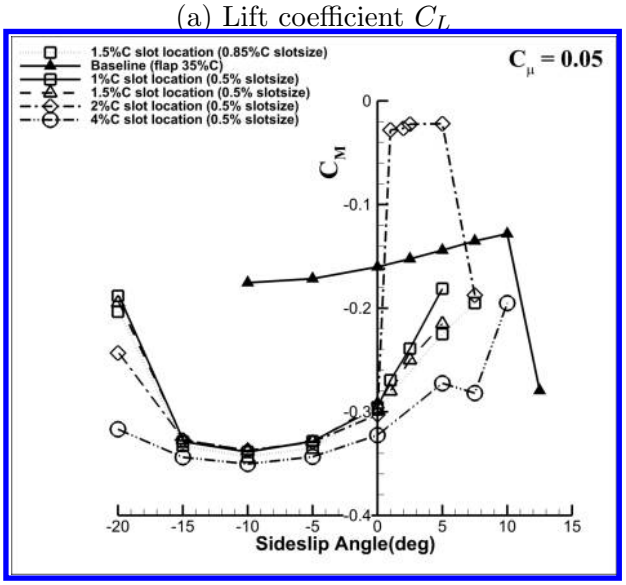

(c) Pitching moment coefficient C_M

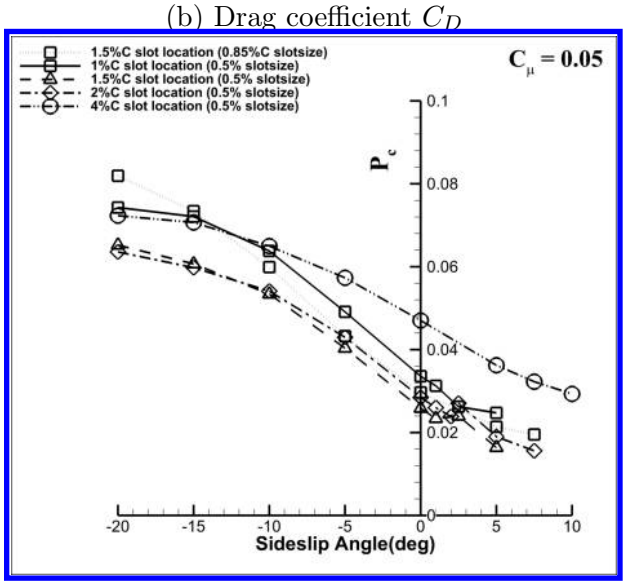

(d) Power coefficient P_c

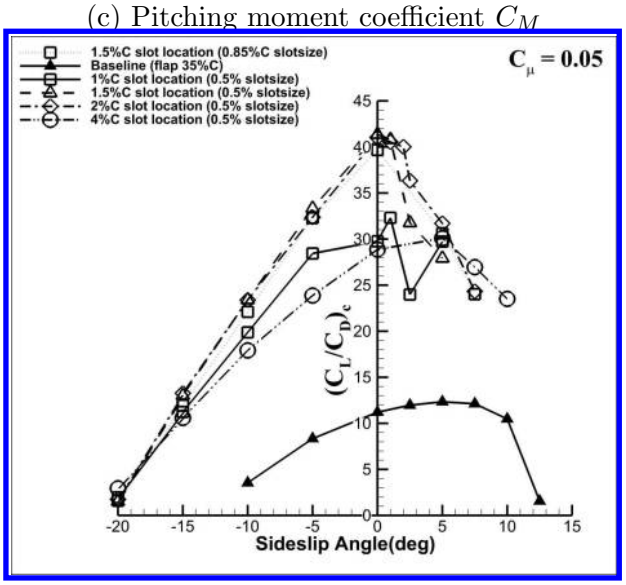

(e) Corrected aerodynamic efficiency $(C_L/C_D)_c$

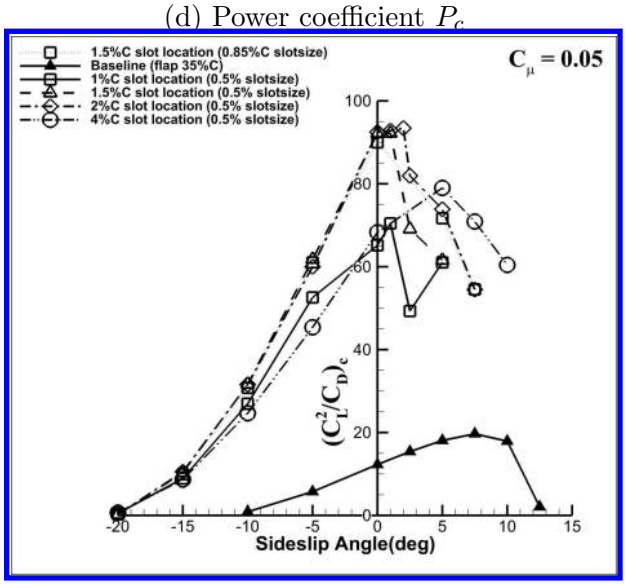

(f)Corrected productivity efficiency coefficient $(C_L^2/C_D)_c$

Figure 8: Aerodynamic coefficients of baseline and CFJ airfoil with injection slot location variation for C_μ=0.05.

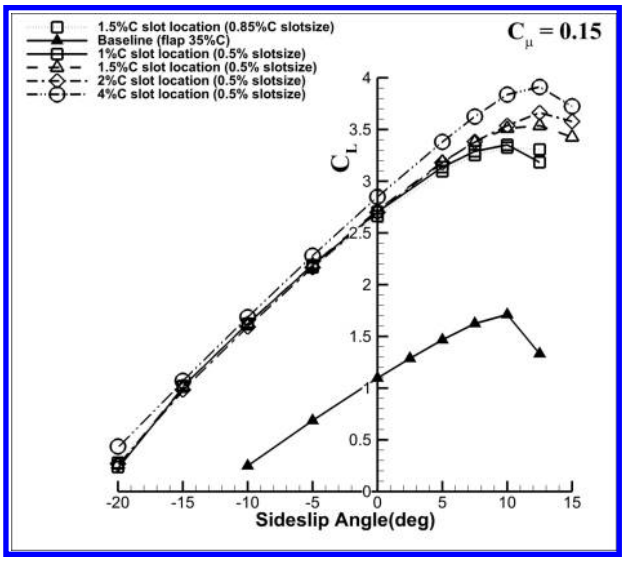

(a) Lift coefficient C_L

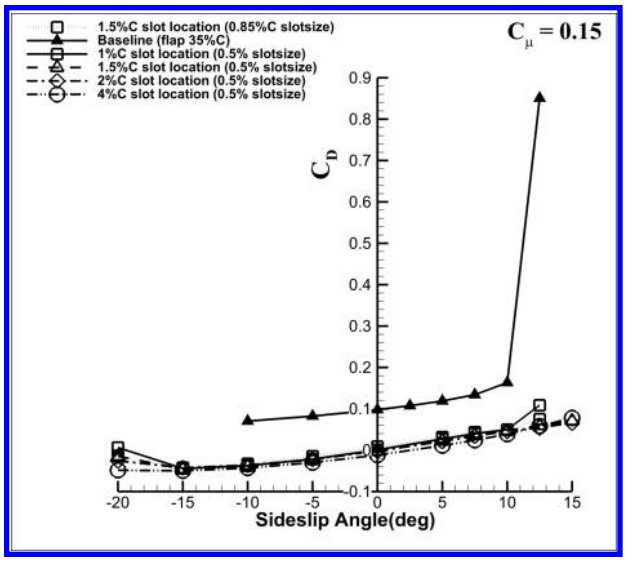

(b) Drag coefficient C_D

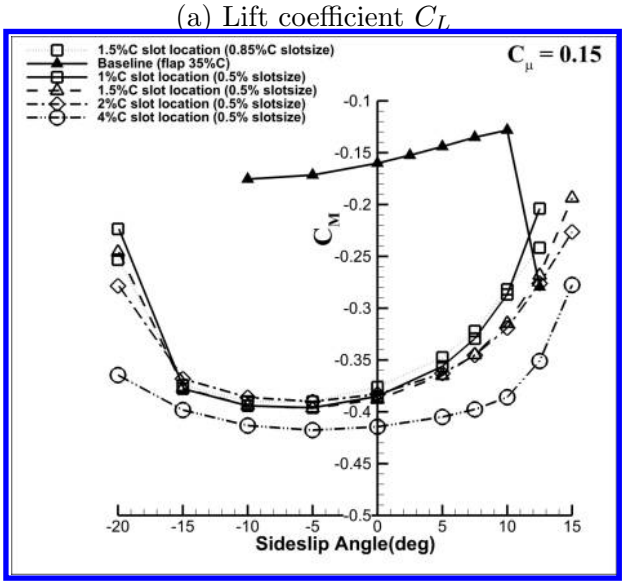

(c) Pitching moment coefficient C_M

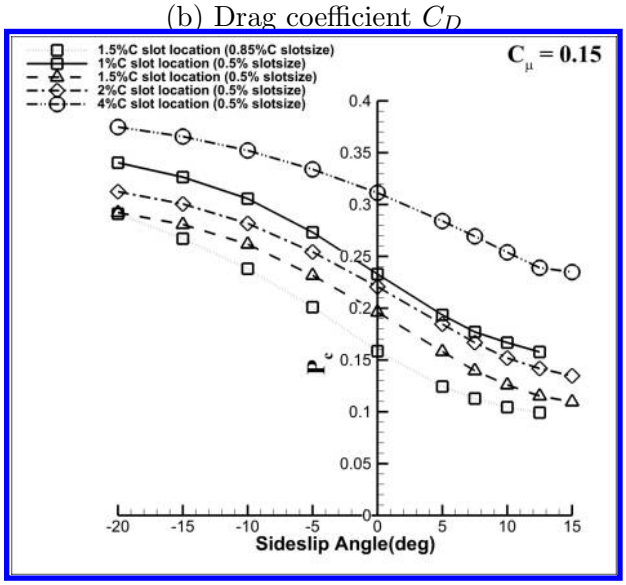

(d) Power coefficient P_c

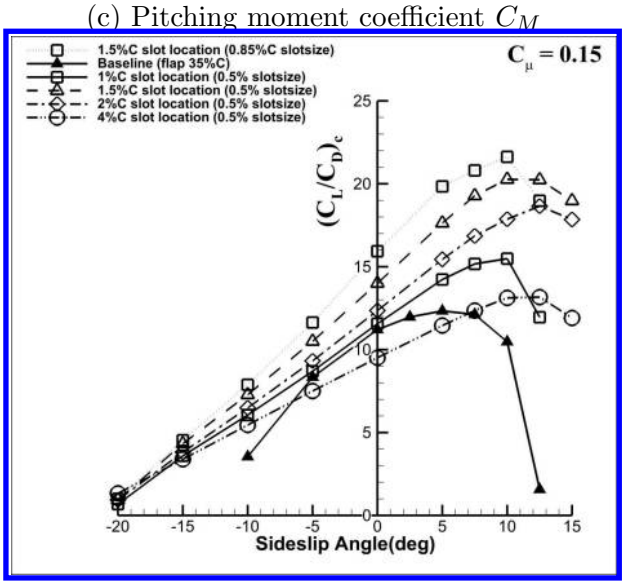

(e) Corrected aerodynamic efficiency $(C_L/C_D)_c$

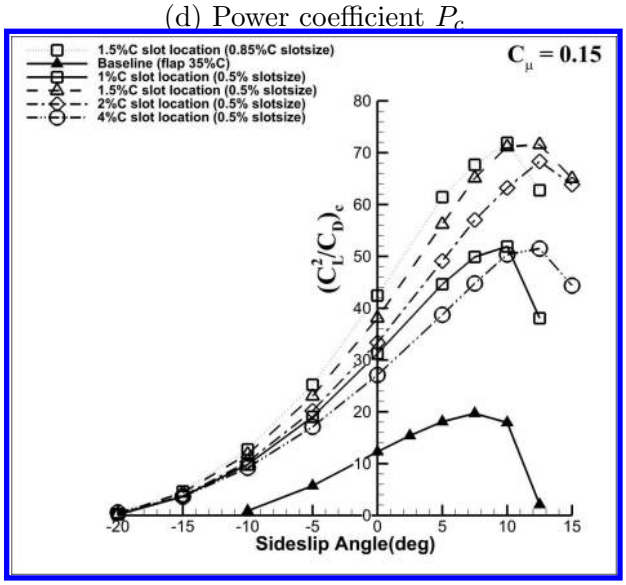

(f)Corrected productivity efficiency coefficient $(C_L^2/C_D)_c$

Figure 9: Aerodynamic coefficients of baseline and CFJ airfoil with injection slot location variation for C_μ=0.15.

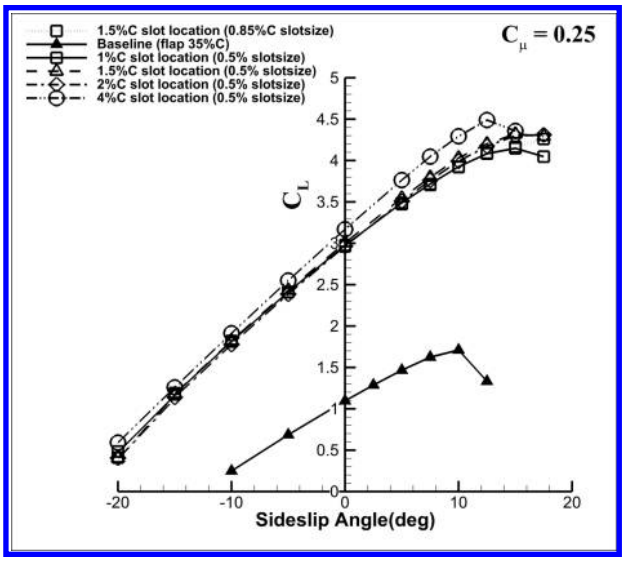

(a) Lift coefficient C_L

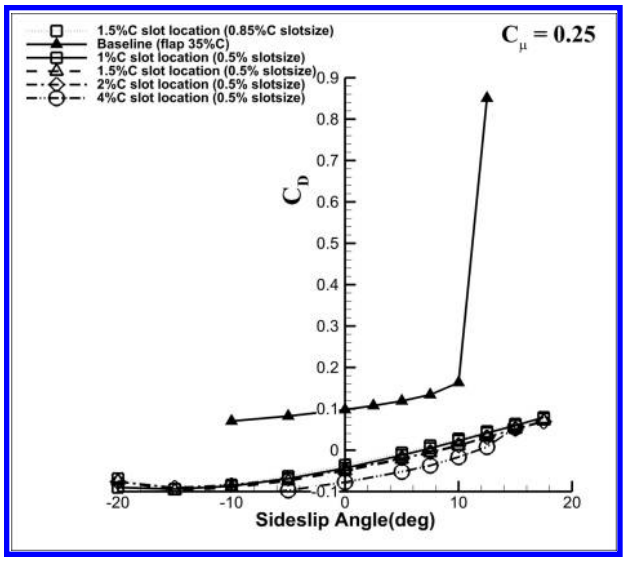

(b) Drag coefficient C_D

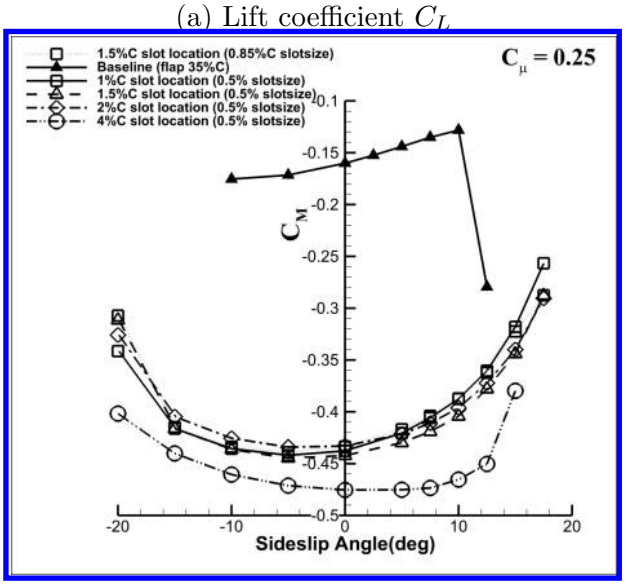

(c) Pitching moment coefficient C_M

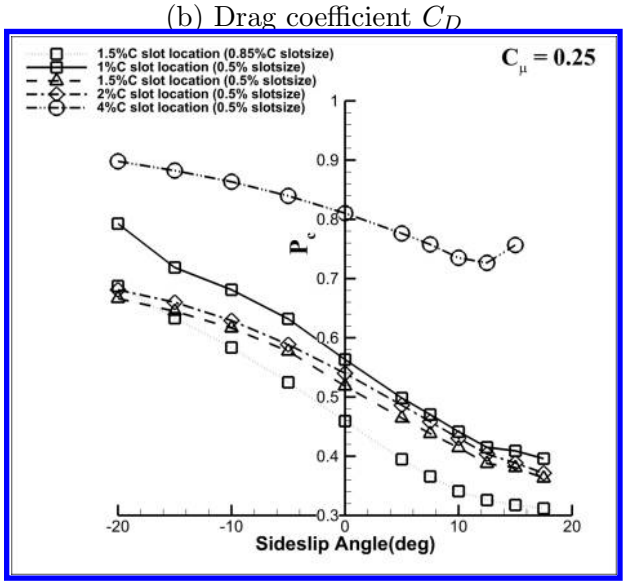

(d) Power coefficient P_c

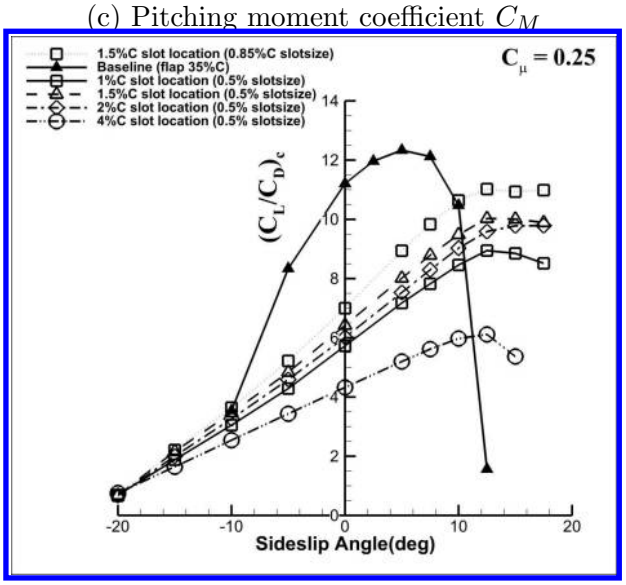

(e) Corrected aerodynamic efficiency $(C_L/C_D)_c$

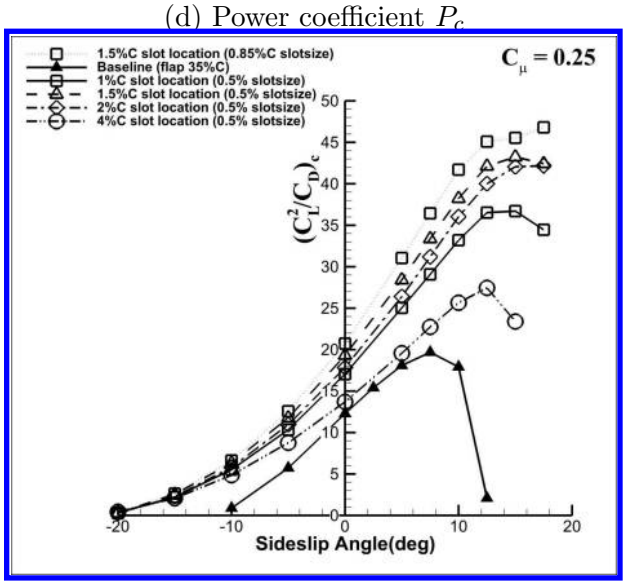

(f)Corrected productivity efficiency coefficient $(C_L^2/C_D)_c$

Figure 10: Aerodynamic coefficients of baseline and CFJ airfoil with injection slot location variation for C_μ=0.25.

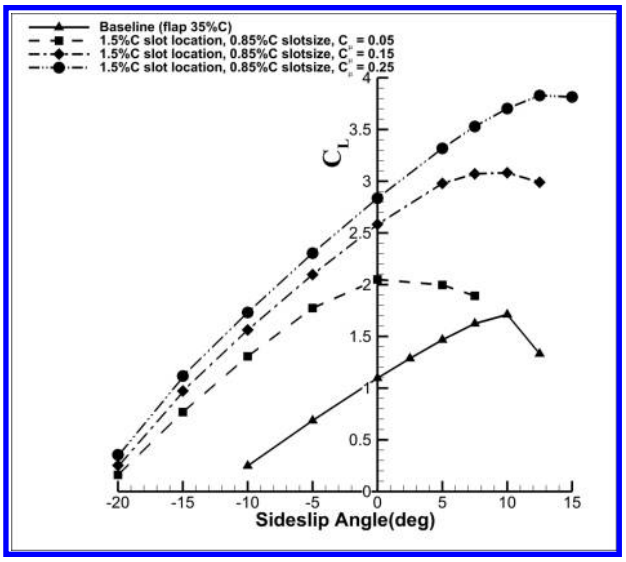

(a) Lift coefficient C_L

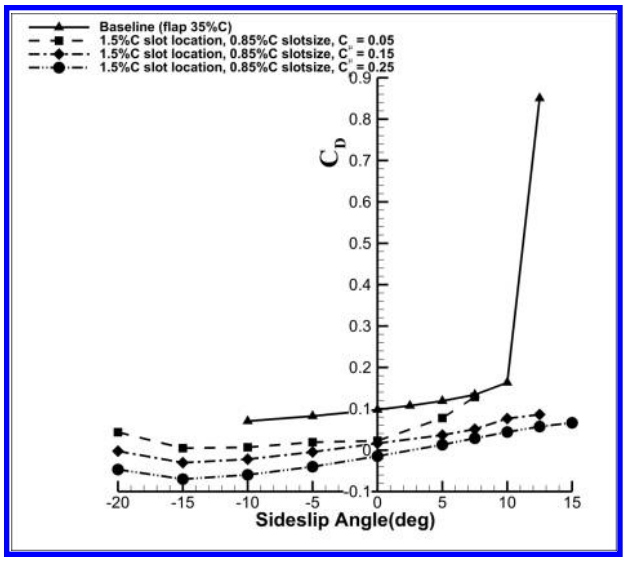

(b) Drag coefficient C_D

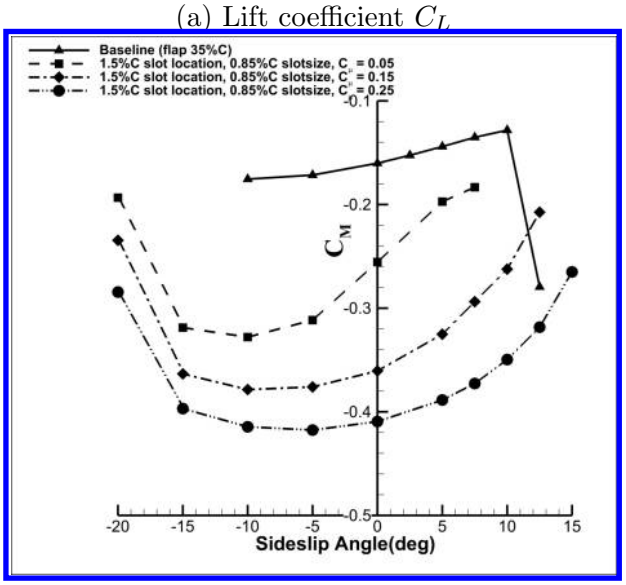

(c) Pitching moment coefficient C_M

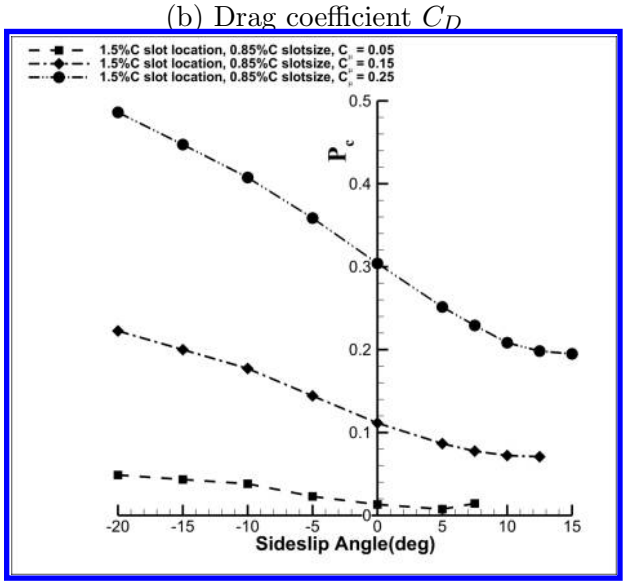

(d) Power coefficient P_c

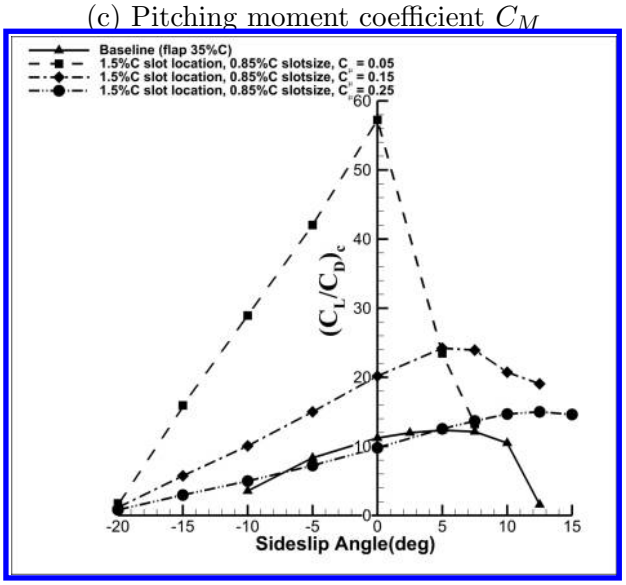

(e) Corrected aerodynamic efficiency $(C_L/C_D)_c$

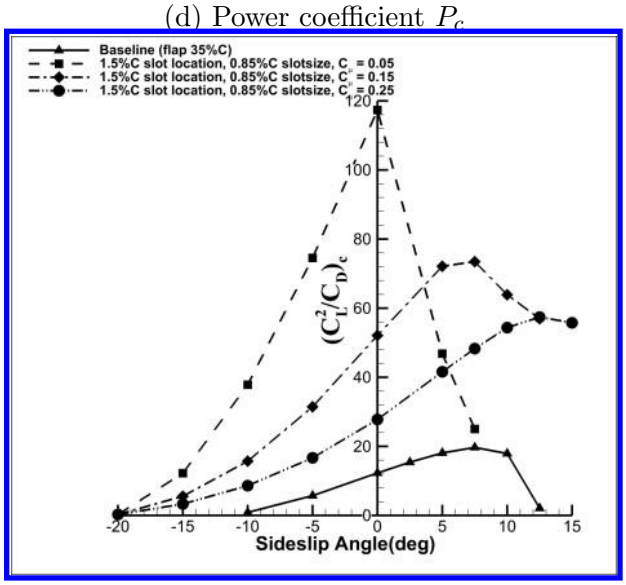

(f)Corrected productivity efficiency coefficient $(C_L^2/C_D)_c$

Figure 11: Aerodynamic coefficients comparison between baseline and optimum CFJ control surface at C_μ=0.05, 0.15, 0.25.

4.2 Inactive CFJ Control Surface at Cruise Conditions

At cruise when the control surface is inactive, the slots may increase drag. To decrease the loss generated by an inactive CFJ system, three methods are studied. One is to let CFJ produce a very light jet at the airfoil surface to fill the slots and reduce the drag at a very low power. The second method is to use a small segment of moving surface to cover the injection and suction slot when CFJ is not in use. The third method is to simply shut down the micro-compressors and leave the CFJ ducts open.

Fig.12 illustrates how the moving surface works during inactive CFJ conditions. For injection slot, when the CFJ is not activated, the moving surface uses point A as a pivot and rotates from point C to B so that injection slot is covered. When the CFJ is activated, the plate will rotate back from B to C and forms the injection slot. For suction slot when CFJ is not activated, a plate embedded beneath the suction surface will slide out from point E to point F to cover suction slot when CFJ is not activated. When the two slots are covered, the control surface airfoil is restored to a similar configuration to the original NACA0012 airfoil and the drag coefficient is also expected to be about the same.

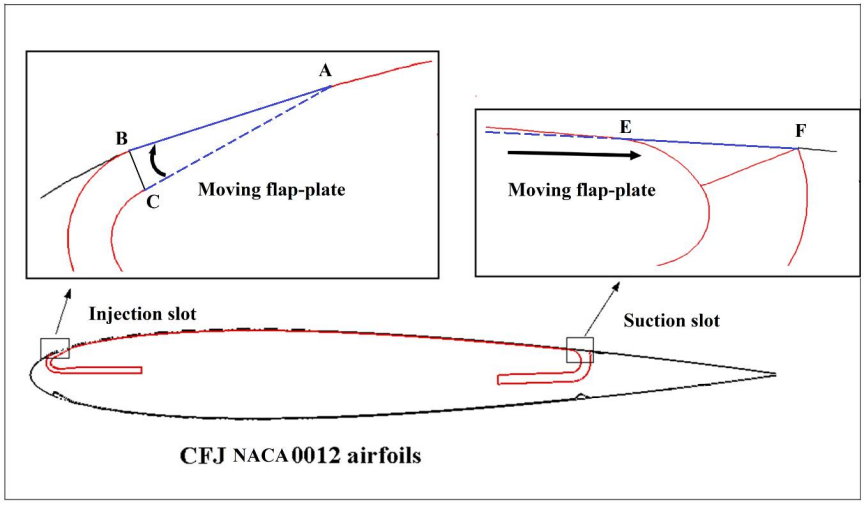

Figure 12: Schematic of moving flap-plate.

Simulations are conducted to evaluate the efficiency of the three methods at Angle of Attack(AoA) of 0° with different cruise Mach number (Ma_∞) of 0.15, 0.45 and 0.7. To compare with the drag coefficient of the baseline control surface with no CFJ, the corrected drag coefficient ($(C_D)_c$) that combines C_D and P_c, will be used as the measure of merit and is defined below:

$$(C_D)_c = C_D + P_c \tag{11}$$

Table 1-3 compares the results of the three methods with baseline NACA0012 at different cruise speed. In each table: Case 1 is the baseline NACA0012; Case 2 is the CFJ-NACA0012 airfoil with the micro-compressor turned off but with the ducts remain open; Case 3 is the CFJ-NACA0012 airfoil with the CFJ and slots covered by moving flap-surfaces; Cases 4-6 are the CFJ-NACA0012 with light co-flow jets.

The conclusion drawn from table 1-3 is that for the method 1 with a light jet, the corrected drag coefficient (C_{Dc}) reduction ranges from 7.5% to 14.6%. For method 2 with the CFJ slots covered, the drag coefficient is

basically the same as the baseline control surface. For method 3 with the micro-compressor turned off, the drag coefficient is increased from 17% at Mach number of 0.15 to 12% at Mach number of 0.7. Note that if the drag coefficient is the same, the total drag is actually reduced since the control surface area will be decreased due to the higher side force lift coefficient of the CFJ vertical tail. Even for the method 3 with the drag coefficient increased, the system may still gain more efficiency if the area reduction is more than the drag coefficient increase.

Fig. 13-15 are the Mach number contours of the airfoils for the above cases at different cruise speed. In all the flow conditions, when the micro-compressors inlet and outlet are closed to mimic the turned off micro-compressor (Case 2), the flow inside the ducts is dominated by recirculated "dead" flow and drag is increased. For case 3 with the slots covered by the moving surfaces, the Mach number contours shown in Fig. 13, 14 and 15 are virtually identical to those of the baseline NACA0012 airfoil. So is the drag coefficient as indicated in table 1-3. Very encouraging results are produced by using very light co-flow jet as shown in table 3 that case 4, case 5, case 6 have the corrected drag coefficient reduced by 13.0%, 14.6% and 11.9% at the transonic speed. Fig. 15d shows the Mach number contour of the CFJ-NACA0012 airfoil with a light co-flow jet at C_μ=0.0025. Similar features of drag reduction and flow phenomenon are also observed at different cruise Mach number of 0.15 and 0.45 as shown in Fig. 13 and Fig. 14. The light jet method reduces corrected drag coefficient by 11.4% at Ma_∞=0.15 and 13.0% at Ma_∞=0.45 condition.

Table 1: $(C_D)_c$ Comparison of Different CFJ Airfoil with Inactive CFJ at Ma_∞=0.15.

Case	Feature	C_D	P_c	V_j/V_∞	$(C_D)_c$	$\Delta(C_D)_c$
1	Baseline	0.0100	-	-	0.0100	0
2	Compressor inlet/outlet closed	0.0117	-	-	0.0117	17.0%
3	Slots covered by moving surfaces	0.0101	-	-	0.0101	1.00%
4	CFJ on, C_μ=0.002	0.00951	-0.00048	0.415	0.00903	-9.75%
5	CFJ on, C_μ=0.0035	0.00809	0.00077	0.551	0.00886	-11.4%
6	CFJ on, C_μ=0.005	0.00673	0.00253	0.659	0.00925	-7.50%

Table 2: $(C_D)_c$ Comparison of Different CFJ Airfoil with Inactive CFJ at Ma_∞=0.45.

Case	Feature	C_D	P_c	V_j/V_∞	$(C_D)_c$	$\Delta(C_D)_c$
1	Baseline	0.0101	-	-	0.0101	0
2	Compressor inlet/outlet closed	0.0113	-	-	0.0113	11.9%
3	Slots covered by moving surfaces	0.0101	-	-	0.0101	0
4	CFJ on, C_μ=0.0015	0.00959	-0.00065	0.371	0.00894	-11.1%
5	CFJ on, C_μ=0.0025	0.00876	-0.00001	0.476	0.00875	-13.0%
6	CFJ on, C_μ=0.0045	0.00706	0.00215	0.632	0.00921	-8.46%

Table 3: $(C_D)_c$ Comparison of Different CFJ Airfoil with Inactive CFJ at Ma_∞=0.7.

Case	Feature	C_D	P_c	V_j/V_∞	$(C_D)_c$	$\Delta(C_D)_c$
1	Baseline	0.00929	-	-	0.00929	0
2	Compressor inlet/outlet closed	0.0105	-	-	0.0105	12.92%
3	Slots covered by moving surfaces	0.00930	-	-	0.00930	0.13%
4	CFJ on, C_μ=0.0015	0.00849	-0.000414	0.381	0.00808	-13.0%
5	CFJ on, C_μ=0.0025	0.00757	0.000358	0.484	0.00793	-14.6%
6	CFJ on, C_μ=0.0035	0.00671	0.00148	0.565	0.00818	-11.9%

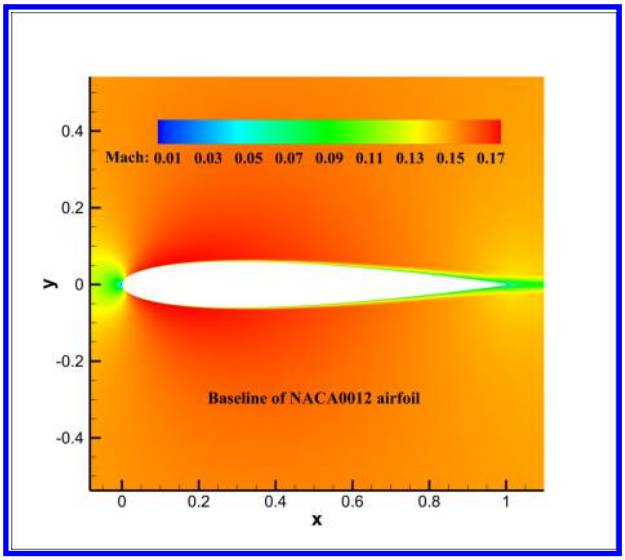

(a) Case 1

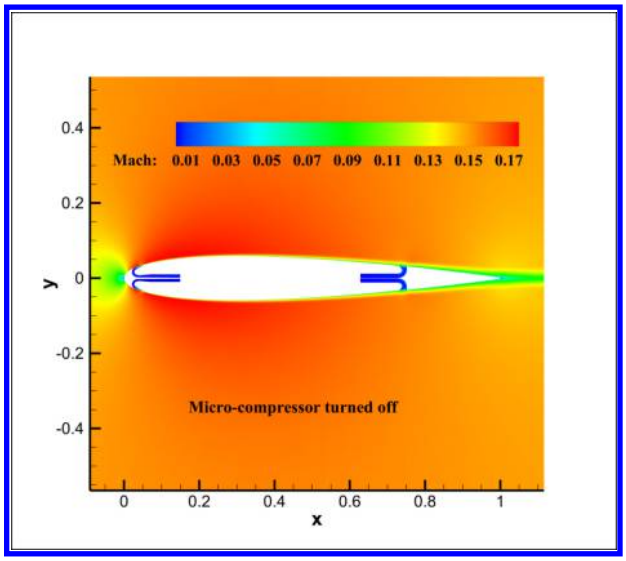

(b) Case 2

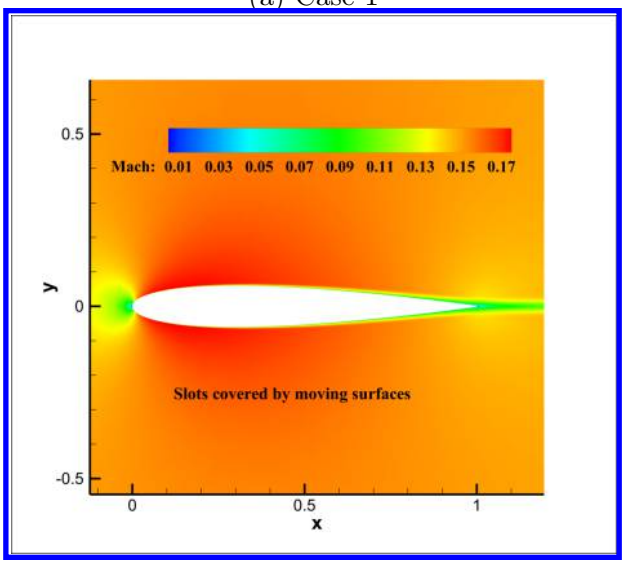

(c) Case 3

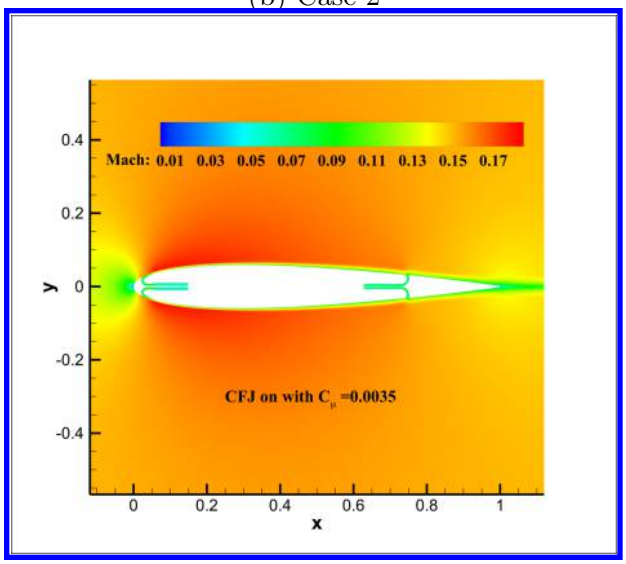

(d) Case 5

Figure 13: Mach number contour of airfoil with inactive CFJ at Ma_∞=0.15.

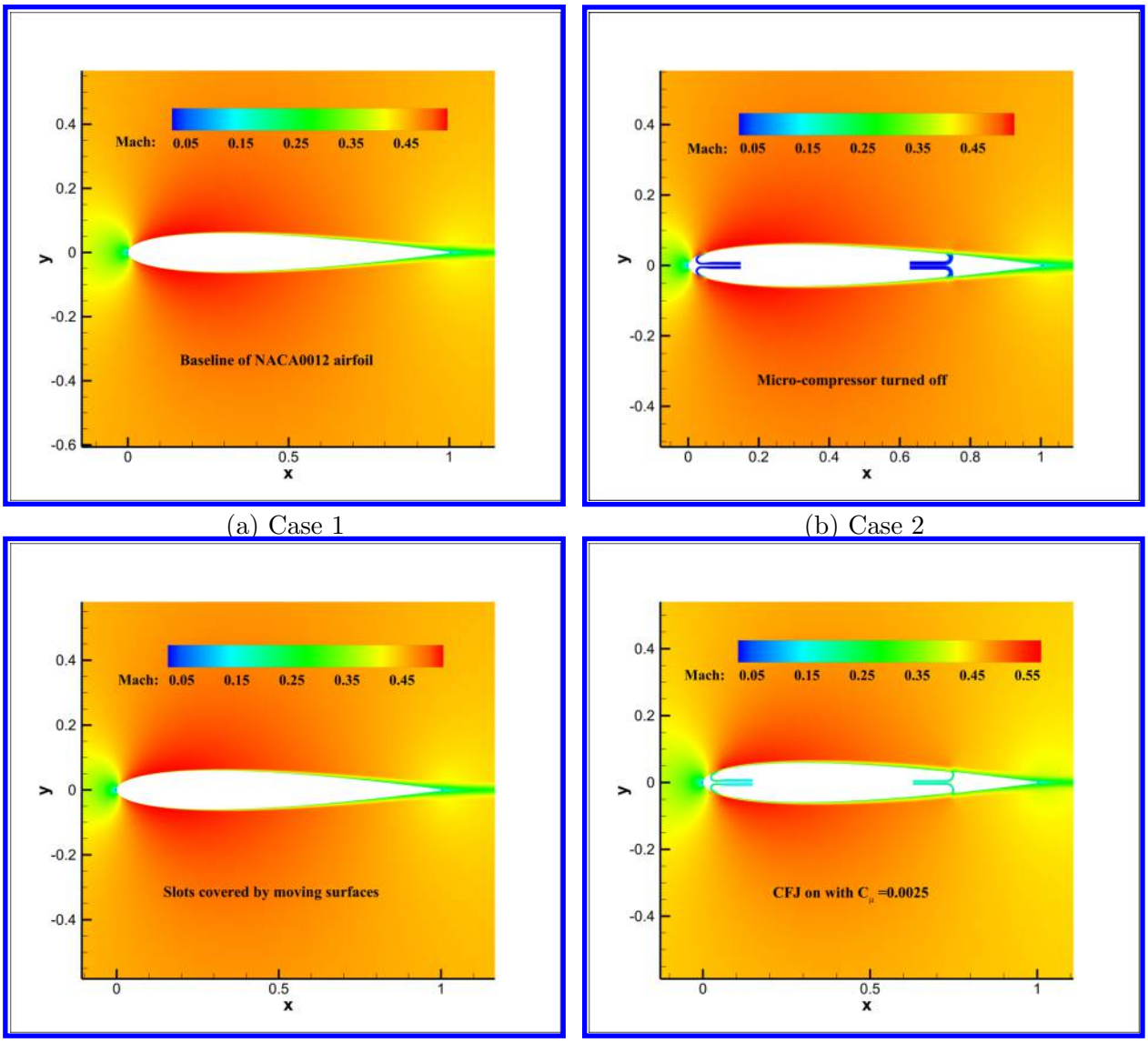

(a) Case 1 (b) Case 2

(c) Case 3 (d) Case 5

Figure 14: Mach number contour of airfoil with inactive CFJ at Ma_∞=0.45.

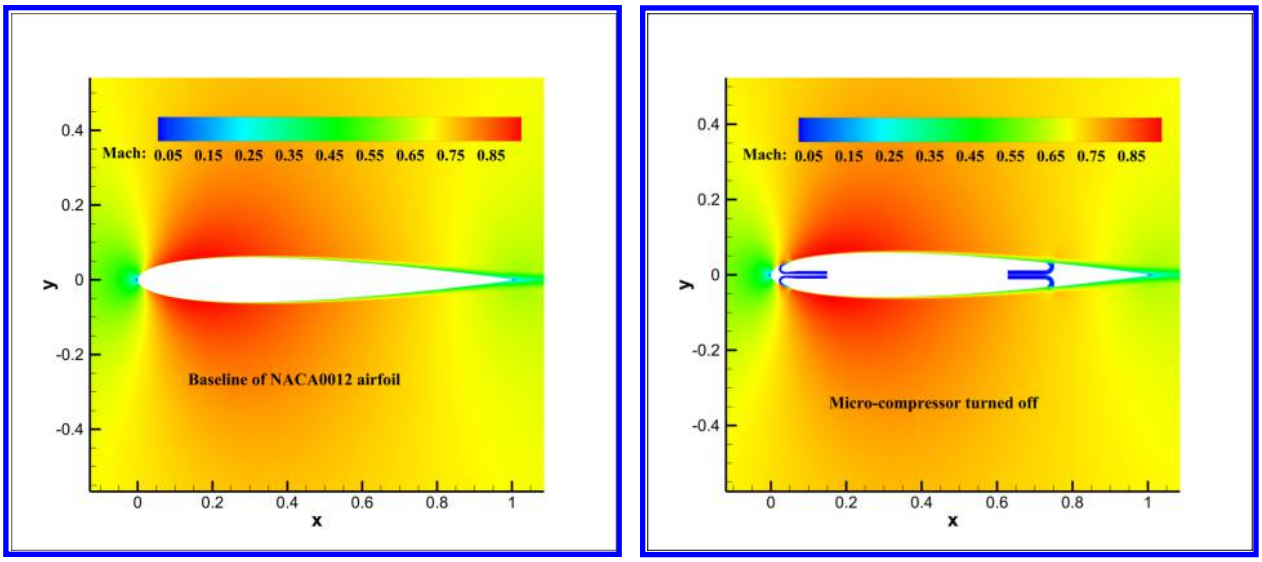

(a) Case 1 (b) Case 2

(c) Case 3 (d) Case 5

Figure 15: Mach number contour of airfoil with inactive CFJ at Ma_∞=0.7.

In summary, both the methods of covering the slots by movable surfaces and using light co-flow jet work very well to reduce the control surface drag at cruise when the control surface is not activated. Each has their pro and con. The pro of the moving surfaces method is that the micro-compressor can be turned off to achieve a long life span. The con is that it needs some moving plates to cover the slots even though they appear to be simple and small. The pro of the maintaining a light CFJ at cruise is that the same airfoil can be used for the whole flight envelope. The con is that the it may decrease the life span of the micro-compressors.

5 Conclusions

This paper numerically investigates drag minimization techniques of the CFJ control surface when it is not activated at cruise condition. Three methods are studied to minimize the control surface drag. One is to let the CFJ produce a very light jet at the airfoil surface to decrease the drag in a low power. This method is effective at various cruise Mach numbers. Compared with the baseline, it decreases the corrected drag coefficient ($(C_D)_c$) by 11.4%, 13.0% and 14.6% at Ma_∞=0.15, 0.45 and 0.7. The second method is to cover the injection and suction slot with a small movable surface segment and turn the CFJ off at cruise. This brings the C_D of CFJ airfoil to the same level as the baseline airfoil. The third method is to simply turn the micro-compressor actuator off and leave the CFJ ducts open with no jet. This method does increase the drag. As a result of the increased lift coefficient that allows reducing the control surface area, the overall drag of the control surface will be significantly decreased. This study indicates that the CFJ control surfaces have great potential to substantially increase the side force for high control authority and reduce total system drag.

6 Acknowledgment

The authors would like to acknowledge the computing resource provided by the Center of Computational Sciences at the University of Miami.

References

[1] S. Anders, W. L. Sellers, and A. Washburn, "Active Flow Control Activities at NASA Langley." AIAA 2004-2623, June 2004.

[2] G.-C. Zha, B. F Carroll, C. D. Paxton, C. A. Conley, and A. Wells, "High-performance airfoil using coflow jet flow control," *AIAA journal*, vol. 45, no. 8, pp. 2087–2090, 2007.

[3] V. Kibens and W. W. Bower, "An Overview of Active Flow Control Applications at The Boeing Company." AIAA 2004-2624, June 2004.

[4] O. Kandil, E. Gercek, X. Zheng, and X. Luo, "Development of computational sensing and active flow control of airfoils during dynamic stall," in *42nd AIAA Aerospace Sciences Meeting and Exhibit*, p. 43, 2004.

[5] A. Lefebvre, B. Dano, W. Bartow, M. Fronzo, and G. Zha, "Performance and energy expenditure of coflow jet airfoil with variation of mach number," *Journal of Aircraft*, vol. 53, no. 6, pp. 1757–1767, 2016.

[6] T. Van Buren and M. Amitay, "Comparison between finite-span steady and synthetic jets issued into a quiescent fluid," *Experimental Thermal and Fluid Science*, vol. 75, pp. 16–24, 2016.

[7] L. Pack, N. Schaeffler, C. Yao, and A. Seifert, "Active control of flow separation from the slat shoulder of a supercritical airfoil," in *1st Flow Control Conference*, p. 3156, 2002.

[8] N. W. Rathay, M. J. Boucher, M. Amitay, and E. Whalen, "Performance enhancement of a vertical tail using synthetic jet actuators," *AIAA Journal*, vol. 52, no. 4, pp. 810–820, 2014.

[9] J. C. Lin, M. Y. Andino, M. G. Alexander, E. A. Whalen, M. A. Spoor, J. T. Tran, and I. J. Wygnanski, "An overview of active flow control enhanced vertical tail technology development," in *54th AIAA Aerospace Sciences Meeting*, p. 0056, 2016.

[10] M. Y. Andino, J. C. Lin, A. E. Washburn, E. A. Whalen, E. C. Graff, and I. J. Wygnanski, "Flow separation control on a full-scale vertical tail model using sweeping jet actuators," in *53rd AIAA Aerospace Sciences Meeting*, p. 0785, 2015.

[11] R. Seele, E. Graff, M. Gharib, L. Taubert, J. Lin, and I. Wygnanski, "Improving rudder effectiveness with sweeping jet actuators," in *6th AIAA Flow Control Conference*, p. 3244, 2012.

[12] R. Seele, E. Graff, J. Lin, and I. Wygnanski, "Performance enhancement of a vertical tail model with sweeping jet actuators," in *51st AIAA Aerospace Sciences Meeting including the New Horizons Forum and Aerospace Exposition*, p. 411, 2013.

[13] N. Rathay, M. Boucher, M. Amitay, and E. Whalen, "Parametric study of synthetic-jet-based control for performance enhancement of a vertical tail," *AIAA Journal*, vol. 52, no. 11, pp. 2440–2454, 2014.

[14] E. Graff, R. Seele, J. C. Lin, and I. Wygnanski, "Sweeping jet actuators-a new design tool for high lift generation," 2013.

[15] A. Shmilovich, Y. Yadlin, and E. Whalen, "Computational evaluation of flow control for enhanced control authority of a vertical tail," *AIAA Journal*, pp. 2211–2220, 2016.

[16] K. Kara, "Numerical simulation of a sweeping jet actuator," in *34th AIAA Applied Aerodynamics Conference*, p. 3261, 2016.

[17] K. Kara, "Numerical study of internal flow structures in a sweeping jet actuator," in *33rd AIAA Applied Aerodynamics Conference*, p. 2424, 2015.

[18] Z. Jinhuan, X. Kewei, Y. Yang, P. P. Ren Yan, and G. Zha, "Aircraft control surfaces using co-flow jet active flow control airfoil," *AIAA Aviation and Aeronautics Forum and Exposition 2018*, 2018.

[19] G. Zha, W. Gao, and C.D. Paxton, "Jet Effects on Co-Flow Jet Airfoil Performance," *AIAA Journal*, vol. 45, pp. 1222–1231, 2007.

[20] G.-C. Zha, C. Paxton, A. Conley, A. Wells, nd B. Carroll, "Effect of Injection Slot Size on High Performance Co-Flow Jet Airfoil," *AIAA Journal of Aircraft*, vol. 43, pp. 987–995, 2006.

[21] Yang, Yunchao and Zha, Gecheng, "Super-Lift Coefficient of Active Flow Control Airfoil: What is the Limit?," *AIAA Paper 2017-1693, AIAA SCITECH2017, 55th AIAA Aerospace Science Meeting, Grapevine, Texas*, p. 1693, 9-13 January 2017.

[22] B.-Y. Wang, B. Haddoukessouni, J. Levy, and G.-C. Zha, "Numerical Investigations of Injection Slot Size Effect on the Performance of Co-Flow Jet Airfoil." AIAA Paper 2007-4427, 2007.

[23] B. P. E. Dano, D. Kirk, and G.-C. Zha, "Experimental Investigation of Jet Mixing Mechanism of Co- Flow Jet Airfoil." AIAA-2010-4421, 5th AIAA Flow Control Conference, Chicago, IL, 28 Jun - 1 Jul 2010.

[24] B. Dano, G. Zha, and M. Castillo, "Experimental study of co-flow jet airfoil performance enhancement using discreet jets," 2011.

[25] Lefebvre, A. and Zha, G.-C. , "Design of High Wing Loading Compact Electric Airplane Utilizing Co-Flow Jet Flow Control." AIAA Paper 2015-0772, AIAA SciTech2015: 53nd Aerospace Sciences Meeting, Kissimmee, FL, 5-9 Jan 2015.

[26] Lefebvre, A. and Dano, B. and Bartow, W. and Di Franzo, M. and Zha, G.-C., "Performance Enhancement and Energy Expenditure of Co-Flow Jet Airfoil with Variation of Mach Number." AIAA Paper 2013-0490, AIAA Journal of Aircraft, DOI: 10.2514/1.C033113, 2016.

[27] Liu, Z.-X. and Zha, G.-C., "Transonic Airfoil Performance Enhancement Using Co-Flow Jet Active Flow Control." AIAA Paper 2016-3066, AIAA Aviation, June 13-17 2016.

[28] Lefebvre, A. and Zha, G.-C., "Trade Study of 3D Co-Flow Jet Wing for Cruise Performance." AIAA Paper 2016-0570, AIAA SCITECH2016, AIAA Aerospace Science Meeting, San Diego, CA, 4-8 January 2016.

[29] X. Kewei and G. Zha, "High control authority 3d aircraft control surfaces using co-flow jet," *AIAA Aviation and Aeronautics Forum and Exposition 2019*, 2019.

[30] G.-C. Zha, W. Gao, and C. Paxton, "Jet Effects on Co-Flow Jet Airfoil Performance," *AIAA Journal, No. 6,*, vol. 45, pp. 1222–1231, 2007.

[31] Yunchao Yang and Gecheng Zha, "Super-Lift Coefficient of Active Flow Control Airfoil: What is the Limit?." AIAA Paper 2017-1693, AIAA SCITECH2017, 55th AIAA Aerospace Science Meeting, Grapevine, January 9-13 2017.

[32] P. Spalart and S. Allmaras, "A One-equation Turbulence Model for Aerodynamic Flows." AIAA-92-0439, 1992.

[33] Shen, Y.Q., and Zha, G.C., "Large Eddy Simulation Using a New Set of Sixth Order Schemes for Compressible Viscous Terms," *Journal of Computational Physics*, vol. 229, pp. 8296–8312, doi:10.1016/j.jcp.2010.07.017, 2010.

[34] G.-C. Zha, Y. Shen, and B. Wang, "An improved low diffusion E-CUSP upwind scheme ," *Journal of Computer & Fluids*, vol. 48, pp. 214–220, 2011.

[35] Y.-Q. Shen, G.-C. Zha, and B.-Y. Wang, "Improvement of Stability and Accuracy of Implicit WENO Scheme ," *AIAA Journal*, vol. 47, pp. 331–344, 2009.

[36] Shen, Y.-Q. and Zha, G.-C. and Chen, X.-Y., " High Order Conservative Differencing for Viscous Terms and the Application to Vortex-Induced Vibration Flows," *Journal of Computational Physics*, vol. 228(2), pp. 8283–8300, 2009.

[37] Shen, Y.-Q. and Zha, G.-C. , " Improvement of the WENO Scheme Smoothness Estimator," *International Journal for Numerical Methods in Fluids*, vol. DOI:10.1002/fld.2186, 2009.

[38] G.-C. Zha and E. Bilgen, "Numerical study of three-dimensional flows using unfactored upwind-relaxation sweeping algorithm," *Journal of Computational Physics*, vol. 125, no. 2, pp. 425–433, 1996.

[39] B. Wang, and G.C. Zha, "A General Sub-domain Bboundary Mapping Procedure for Structured Grid CFD Parallel Computation." AIAA Paper 2007-4432, 2007.

[40] Wang, B.-Y. and Haddoukessouni, B. and Levy, J. and Zha, G.-C., "Numerical Investigations of Injection Slot Size Effect on the Performance of Co-Flow Jet Airfoil," *Journal of Aircraft*, vol. Vol. 45, No. 6,, pp. pp.2084–2091, 2008.

[41] Wang, B. Y and Zha, G.-C. , "Detached-Eddy Simulation of a Co-Flow Jet Airfoil at High Angle of Attack." AIAA Paper 2009-4015, accepted for publication in Journal of Aircraft, 2011.

[42] Im, H.-S. and Zha, G.-C. and Dano, B. P. E., "Large Eddy Simulation of Coflow Jet Airfoil at High Angle of Attack," *Journal of Fluid Engineering, vol. 136(2), p. 021101*, 2014.

[43] C. L. Ladson, A. S. Hill, and W. G. Johnson Jr, "Pressure distributions from high reynolds number transonic tests of an naca 0012 airfoil in the langley 0.3-meter transonic cryogenic tunnel," 1987.